Appl Phys B (2010) 100: 461–469
DOI 10.1007/s00340-010-4076-9

Applied Physics B
Lasers and Optics

A compact, quasi-monochromatic laser-plasma EUV source based on a double-stream gas-puff target at 13.8 nm wavelength

P.W. Wachulak · A. Bartnik · H. Fiedorowicz · T. Feigl ·
R. Jarocki · J. Kostecki · R. Rakowski · P. Rudawski ·
M. Sawicka · M. Szczurek · A. Szczurek · Z. Zawadzki

Received: 10 November 2009 / Revised version: 27 April 2010 / Published online: 22 May 2010

Abstract A compact, high-repetition table-top EUV source, based on a gas-puff target, is presented. This source was developed in our group and is capable of emitting quasi-monochromatic radiation at 13.8 nm wavelength with the inverse relative bandwidth of 140 and pulse energies up to ∼1.3 μJ/pulse at 10-Hz repetition rate. The source is debris-free, operates near the lithographic wavelengths and offers the energy density of ∼0.4 mJ/cm^2 in each EUV pulse. These three features make the source attractive for lithographic experiments. The timing optimization of the source, its energy per pulse, spectral and spatial distributions are pointed out in detail as well as the enhancement in energy density achievable with a multi-layer collector mirror compared to a planar mirror of equal reflectivity.

1 Introduction

The recent development of compact short-wavelength sources has promoted the study of matter properties in the EUV regime. The strong demand for such quasi-monochromatic sources results from the semiconductor industry striving for even smaller, faster and less power consuming computer chips. Compact EUV sources give the opportunity to perform the experiments without the necessity to employ large "photon facilities" with limited user access. Thus these sources have a huge impact on the speed of the EUV technology development since the experiments are now not restricted to large facilities only, but can be performed in the lab environment, quicker, cheaper and with similar results. Moreover, the importance of the development and the commercial availability of the EUV sources, in particular the lack of commercial tools for actinic inspection, for the semiconductor industry, was already noted by Intel [1]. The usability of the existing EUV sources was proved by many examples of the experiments involving compact table-top EUV sources such as capillary discharge lasers for the Interferometric Lithography IL and wavelength resolution holography [2, 3], high-harmonic generation sources [4, 5] for the lens-less imaging [6] and surface deformation studies [7], optically pumped EUV lasers in the EUV microscopy with the use of zone-plates [8], xenon discharge produced plasma (DPP) EUV source from Energetic used for development of actinic full-field EUV mask blank inspection tool at MIRAI-Selete [9] and many more.

One of these compact sources is a gas-puff target EUV source. The suitability of gas-puff target for an efficient soft X-ray generation in the "water window" range was demonstrated, resulting in strong line emission from the 1–2 transitions in H-and He-like nitrogen ions at $\lambda = 2.478$ nm and 2.879 nm, respectively using 5 J energy per pulse Nd:glass laser for an excitation [10] or recently in a very compact, table-top setup employing much smaller Nd:YAG, 0.74 J energy per pulse laser [11]. A significant enhancement of X-ray production in the 1-keV energy range was achieved by

---

P.W. Wachulak (✉) · A. Bartnik · H. Fiedorowicz · R. Jarocki ·
J. Kostecki · R. Rakowski · P. Rudawski · M. Szczurek ·
A. Szczurek · Z. Zawadzki
Institute of Optoelectronics, Military University of Technology,
ul. gen. S. Kaliskiego 2, 00-908 Warsaw, Poland
e-mail: wachulak@gmail.com
Fax: +48-22-6668950

T. Feigl
Fraunhofer Institut für Angewandte Optik und Feinmechanik
(IOF), Albert-Einstein-Str. 7, 07745 Jena, Germany

M. Sawicka
Department of X-ray Lasers, Institute of Physics/ PALS Centre,
Academy of Sciences of the Czech Republic, Na Slovance 2,
182 21 Prague 8, Czech Republic

modification of a single nozzle gas-puff target to a double-stream gas-puff target [12]. Employing X-ray radiation, in the wavelength range from 6 to 20 nm, produced as a result of irradiation of a double-stream gas-puff target with Nd:YAG laser, a direct and very efficient photo-etching of PTFE polymer was reported [13]. Gas-puff target EUV source was also used for studying a fluorescence radiation in the EUV from Al and Si [14] and micro-structuring of PMMA polymer [15]. It was also shown that employing a double-stream gas-puff target the energy conversion efficiency from IR pumping laser to EUV radiation emitted near the 13.5 nm band may be significantly improved. The calculated EUV production can be as large as 8.7×10^{13} ph/sr, corresponding to 8 $\mathrm{mJ}/2\pi$ of emitted energy and the conversion efficiency equal to 1.6% [16]. However, for some applications, such as EUV microscopy using diffractive optics for example, a monochromaticity of the EUV radiation, produced using the gas-puff target, is a key parameter that needs to be studied. Thus, in this paper, we report and characterize a compact high-repetition table-top, quasi-monochromatic EUV source, based on a similar double nozzle gas-puff target that might be employed in applications requiring narrow-bandwidth EUV radiation. Using an argon/helium gas-puff and a collinear double-stream electromagnetic valve, an efficient EUV production was achieved in the range between 6 and 20 nm. Employing an elliptical multi-layer mirror (MLM) as a spectral filter and a EUV radiation collector, the bandwidth was drastically narrowed. As a result, an efficient EUV source was developed in our group capable of emitting quasi-monochromatic radiation at 13.8 nm wavelength. Timing optimization of the source, its energy per pulse, spectral and spatial distributions are presented in detail. The enhancement in energy density achievable with a multi-layer collector mirror compared to a planar mirror of equal reflectivity is also investigated.

2 Experimental setup

The experimental setup of the compact gas-puff target EUV source is schematically shown in Fig. 1a and its photograph in Fig. 1b. An infrared laser pulse $\lambda = 1064$ nm with 737 mJ energy and 4 ns time duration from commercial Nd:YAG laser NL 303HT from Eksma, Lithuania was focused using an $f = 25$ mm focal length lens onto a double-stream gas-puff target produced by the electromagnetic double nozzle valve system. The nozzle is composed of a round inner nozzle with a diameter of 0.4 mm and a ring-shaped outer nozzle with diameters of 0.7 and 1.5 mm.

Argon is used as the working gas. To achieve an optimum plasma density further away from the nozzle surface, second low-Z gas (helium) was used to confine the inner gas closer to the nozzle axis to decrease the gradient of the working gas density. The position of the focused IR radiation from the pumping laser was optimized for the highest EUV photon production. For argon this position is ∼0.2–0.3 mm from the axis of the nozzle in the direction of the multilayer mirror. To avoid the nozzle ablation by the plasma, the distance between the nozzle exit and the pumping laser focus was 1.5 mm. The optimum Ar/He pressure was found to be ∼10 bar and 5 bar, respectively. To avoid high gas pressure inside the vacuum chamber containing the experimental setup, a differential pumping was employed maintaining constantly a pressure of 10^{-4}–10^{-2} bar during the tests by two roughing pumps and one turbomolecular pump.

Crucial for an efficient EUV production using a gas-puff target is the proper timing of the nozzles. Three delays need to be adjusted to properly drive the nozzles. The nozzle controller was synchronized with the synchronization output of the pumping laser in order to minimize the jitter in the nozzle time sequence. Time TD1 is the delay between the synchronization pulse from the pumping laser power supply and the opening time of the working gas nozzle, TD2 is the same delay time for the second—outer nozzle, time PW describes the pulse width—time measured from the TD1 time to the

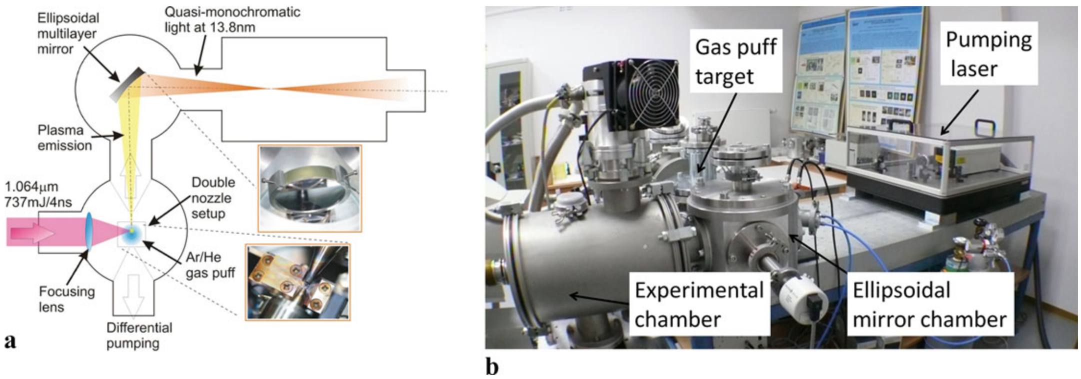

Fig. 1 Scheme of the EUV source with a major components indicated (**a**) and the photograph of the source (**b**)

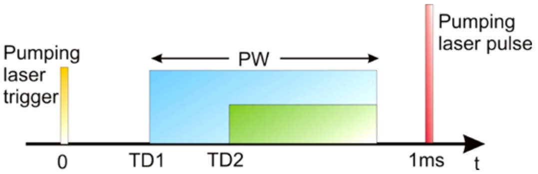

Fig. 2 Schematic description of a double nozzle gas-puff target EUV source delay parameters

point where both valves are closed. The nozzle time parameters are depicted in Fig. 2.

Another very important issue from the efficiency point of view is a proper EUV light collection. As a collector a MLM was used. An 80-mm diameter fused silica mirror substrate was polished to have an ellipsoidal surface with the radii of ∼179.6 mm and 254 mm necessary to limit the spherical aberration of the off-axis optic. The substrate was fabricated by Reflex s.r.o. company, Czech Republic. The multilayers were optimized to give a maximum reflection at the wavelength of 13.5 ± 0.5 nm (FWHM) and the incidence angle of 45°. This was achieved by a stack of 40 silicon and molybdenum layers deposited on the concave substrate. The multi-layer period was equal to 10.05 nm with the γ factor of 0.38 ± 0.02 defined as a ratio of the bottom layer thickness to the multi-layer period. The Si layer (top) thickness is then 6.23 nm and that of Mo layer 3.82 nm. The multilayers were deposited at Fraunhofer Institut für Angewandte Optik und Feinmechanik, Jena, Germany. The theoretical reflectivity of the mirror at 13.5 nm wavelength was found to be 37.75% for unpolarized light, such as the output of the laser-plasma EUV source.

The MLM was designed to image the point-like plasma source to an image plane with a unity lateral magnification, having both the object and image distances equal to 254 mm. From the source the collector appears as an ellipse with radii of 40 and 28.3 mm. The purpose of this optic is two-fold, firstly to collect most of the plasma emission and secondly to spectrally select only the plasma radiation from the MLM reflectivity range of 13–14 nm.

3 Experimental results

During the measurements the optimization of the nozzle timing was performed in order to optimize the number of photons in the range set by the reflection properties of the MLM optic. This optimization was necessary to maximize the peak irradiance at 13.84 nm, strongest Ar line in the wavelength range 13–14 nm. Spectral measurements were performed with and without the collector to show the influence of the spectral selector on the emission spectrum. Spatial distribution of the EUV light at the focal point of the MLM optic was investigated and, finally, the MLM enhancement factor was studied in detail.

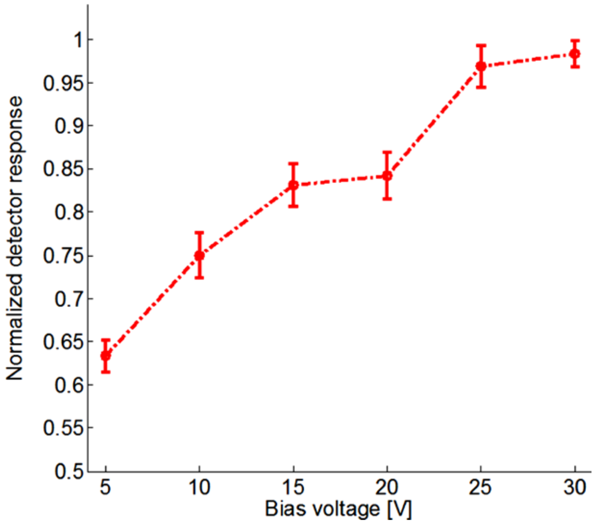

Fig. 3 Normalized AXUV 100 detector response curve vs. detector bias voltage

3.1 Nozzle timing optimization

Optimal emission from the gas-puff laser-plasma source requires optimal timing of the valves. For the measurements an AXUV100 Ti/Zr/C 6/200/50 detector, a silicon p–n junction photodiode from International Radiation Detectors, Inc., was used, coated with a 200-nm thick layer of zirconium to filter out the wavelengths above ∼18 nm [17]. The sensitive area of the detector is 10 × 10 mm^2 in size. The signal from the detector was stored using a 4 GHz Tektronix DPO 70404 oscilloscope and later integrated numerically. At 13.8 nm wavelength the quantum efficiency of the detector was assumed to be 6.9 electrons per photon [18]. It was found in subsequent measurements that the bias voltage necessary to apply to the detector needs to be 25–30 V. For that bias voltage, the response curve of the detector saturates meaning that the influence of the bias voltage to the detector response is minimized. This can be clearly seen in Fig. 3 depicting the normalized detector response as a function of the bias voltage. The experimental arrangement for timing optimization is shown in Fig. 4a.

The influence of the change of three timing parameters TD1, TD2 and PW from the optimum values can clearly be seen in Fig. 5. The pumping laser pulse arrives ∼1 ms after the synchronization pulse. Most important is the TD1 time, since it defines the delay between the synchronization pulse and the activation of the working gas valve. If the delay is too short, the IR pulse excites the gaseous target, which has lower density than optimal, since the valve was opened too early and the working and outer gases were injected into the vacuum chamber for too long time. If the TD1 delay is too long, above 1 ms, the IR pulse arrives before the actuation of the working gas nozzle. The optimum value of the TD1

Fig. 4 Scheme of the experimental arrangement for a source timing optimization (**a**) for maximum photon flux, and (**b**) for peak intensity in the selected by a MLM Ar line

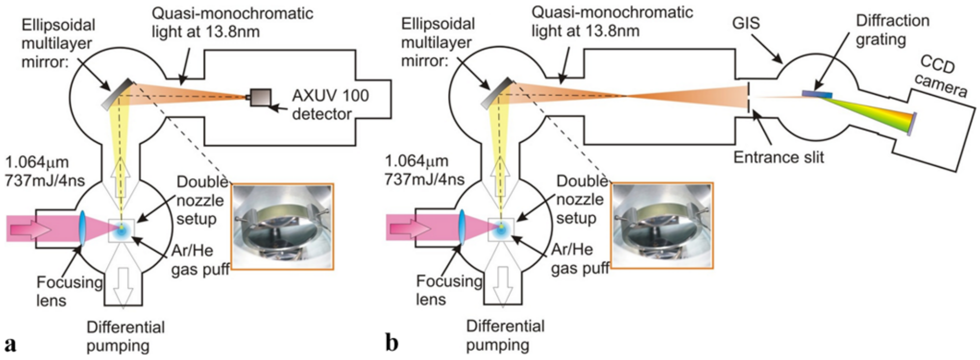

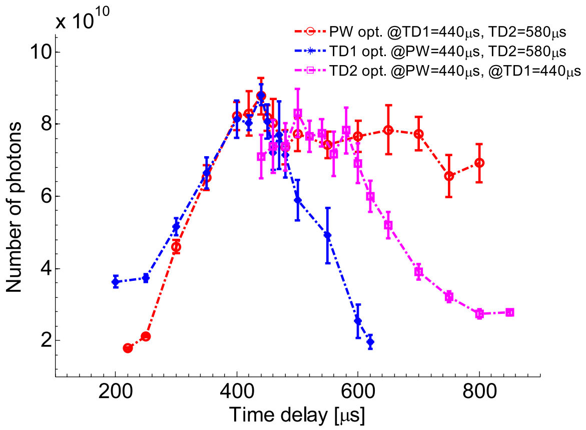

Fig. 5 Number of photons in the wavelength range from 13 to 14 nm as a function of the time delay for three timing parameters TD1, TD2 and PW

delay is when the IR pulse excites the target having the optimal density for efficient EUV generation. When the pulse width is too short the amount of gas injected into the vacuum chamber is too small and the working gas density is lower than the optimal one, while if the PW is too long, the gas density increases and is too high so that an extra absorption of the EUV light occurs, thus the EUV photon production decreases. The working gas valve is usually opened first, so TD1 $<$ TD2. If both valves are opened simultaneously, the efficiency of the EUV photon production decreases from the optimal value. Our investigations suggest to open the outer valve ∼60 μs after the first one. If the TD2 delay is further increased, a situation arises where the IR exciting pulse arrives before the pressure of the outer gas injected to the vacuum chamber is able to shape the density profile of the inner-working gas and the efficiency of the short-wavelength photon production is drastically reduced.

The peak of the EUV photon production was equal to $\sim 8.8 \pm 0.5 \times 10^{10}$ photons per pulse in band—in the wavelength range between 13 and 14 nm. These optimal conditions were achieved for TD1 = 440 μs, PW = 440 μs and TD2 = 580 μs for Ar/He pressures of 10 and 5 bar, respectively. The measurements were taken using the AXUV 100 detector with a Zr filter deposited. The error bars in each point were assessed as a standard deviation based on ten consecutive measurements. That corresponds to 1.29 μJ/pulse and at 10-Hz repetition rate this gives 12.9 μW of power in band.

The timing optimization was also performed for maximum intensity of the Ar 13.84 nm, $2p^63s$–$2p^65p$ transition in the Ar VIII plasma. Highest intensity does not mean highest photon flux, since changing the delays influences slightly the spectral distribution of the EUV radiation generated by the investigated source.

The experimental arrangement for this test is shown in Fig. 4b. The Ar spectra for different timings were measured using a Grazing Incidence Spectrometer (GIS) equipped with a variable groove reflection grating of 1200 lines per millimeter, 25.5 μm entrance slit and 1300 × 400 pixels back-illuminated CCD camera (Princeton Instruments). From the geometry of the spectrometer and the grating used, the inverse relative bandwidth of the spectrometer was estimated to be $\frac{\lambda}{\Delta\lambda} \approx 585$ and at 13.84 nm wavelength the spectral resolution of the spectrometer was equal to 0.24 Å.

The GIS was attached to the source equipped with MLM. Its spectral range was between 6 and 22 nm. The spectra were accumulated over 30 EUV pulses (3 s at 10 Hz repetition rate). For all spectra the background images were subtracted and the spectra were binned vertically. Then the peak intensity was found at the interesting 13.84 nm line and the results were normalized. The change of the timing parameters TD1, TD2 and PW from the optimum values results in an intensity change of the 13.84 nm Ar line. This can be observed in Fig. 6. The error bars in each measurement correspond to a ∼3.7% standard deviation based on ten spectral measurements.

Comparing to Fig. 5, the shape of the curves is similar. As before the strongest dependence occurs for the TD1 delay; however, the highest intensity in the 13.84 nm Ar line is obtained for a slightly different combination of the three time delays: TD1 = 440 μs, PW = 450 μs and TD2 = 580 μs.

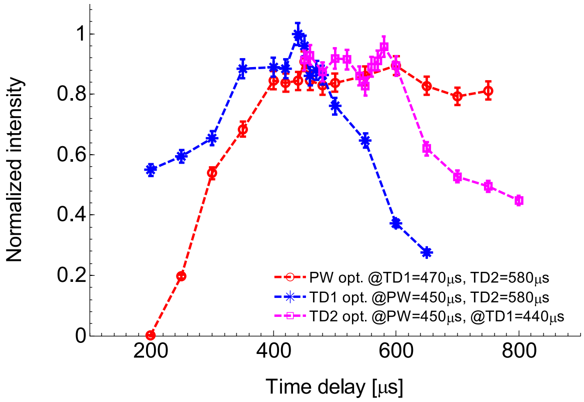

Fig. 6 Normalized intensity as a result of nozzle timing optimization for a maximum intensity in the 13.84 nm Ar line

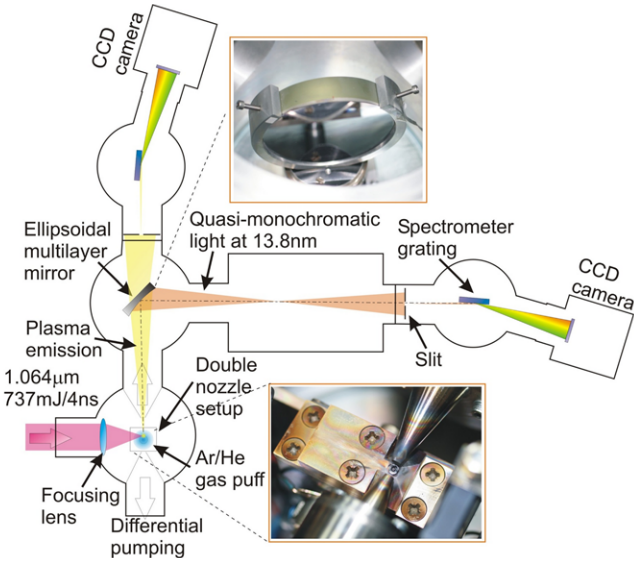

Fig. 7 Schematic of the experimental arrangement for spectral measurements with and w/o the MLM collector

3.2 Spectral distributions of the EUV radiation

The spectral measurements were carried out using the spectrometer described in Sect. 3.1. Both spectra: of the source equipped with a MLM collector and the Ar spectrum were obtained. The scheme of the experimental arrangement is depicted in Fig. 7. To avoid saturation of the 15-bit CCD camera saturation, 8 EUV pulses were necessary to accumulate the Ar spectrum shown in Fig. 8a, b as a dashed line. The spectrum with the MLM employed—solid line, required 30 EUV pulses to accumulate sufficient number of photons. In both measurements the background images were acquired and then subtracted from the spectral measurements in order to minimize the CCD internal noise influence on the measurements. Figure 8a shows both spectra normalized to their peak intensities. Most visible lines were recognized according to [19] and the spectrometer was calibrated by fitting a second-order polynomial curve to translate the pixel value of the CCD to the wavelength. Based on 8 data points, the fitting polynomial was a parabolic function described by the equation $y = 2.15 \times 10^{-6} \cdot x^2 + 9.23 \times 10^{-3} \cdot x + 6.18$, where the y-value is the wavelength expressed in [nm] while x is the horizontal CCD pixel. The correlation with the data points was practically equal to one. Using the MLM reflection curve obtained by simulating the multi-layer Mo/Si stack with the parameters described in Sect. 2, both spectra "in scale" are depicted in Fig. 8b—the solid and dashed lines. The MLM reflection curve is depicted as a dotted line. The most interesting lines in Ar VIII are the transitions $2p^63p$–$2p^65d$ at 13.793 nm and $2p^63s$–$2p^65p$ shifted slightly to the longer wavelength at 13.844 nm. Since there is 0.51 Å spectral separation between these lines, the spectrometer can resolve them. However, this was not possible for the $2p^63s$–$2p^64p$ J–J 1/2–3/2 (15.892 nm) and 1/2–1/2 (15.918 nm) transitions separated by 0.26 Å only. This is the reason why this "double" line dominates the spectrum obtained. A more detailed view of the spectral emission from the EUV source equipped with a MLM in the range of wavelengths from 10–20 nm is shown in Fig. 9. Despite of a very small reflectivity of the MLM outside its operating wavelength range (only a few %), very strong emission lines around 16 and 18 nm are still slightly visible. So to further limit the contribution of these weak lines to the emission spectrum, a 141-nm thick Zr filter was used—dotted line. The result of the filtration is shown as a dashed line in Fig. 9. The inset plot shows in detail the two lines, mentioned above, which are of interest from the point of view of this paper. The relative inverse bandwidth of the filtered emission, shown in Fig. 9, was measured to be $\frac{\lambda}{\Delta\lambda} \approx 140$.

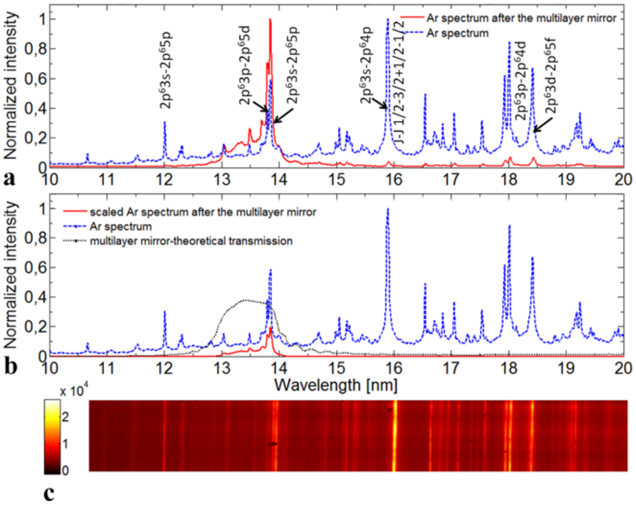

Fig. 8 Spectral measurements of the Ar plasma emission with and without the use of the MLM. Both spectra were normalized (**a**) and most pronounced spectral lines were found. Both spectra are shown "in scale", (**b**) and (**c**) show the spectrum of the Ar plasma obtained using the GIS spectrograph

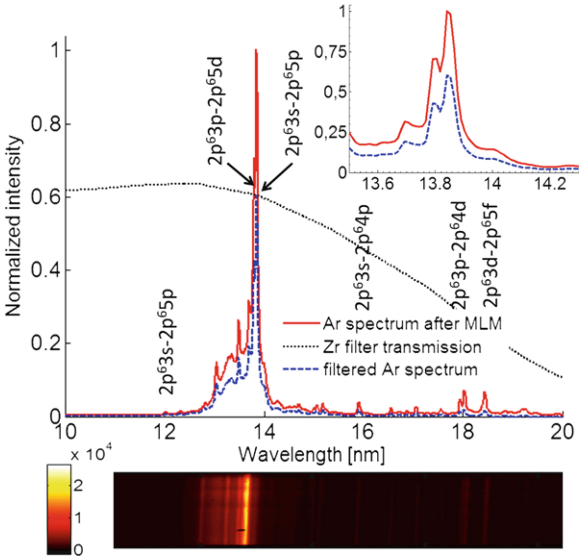

Fig. 9 Detailed view of the spectral emission from the EUV source equipped with a MLM in the wavelength range from 10–20 nm. To further limit the influence of small contribution to the emission spectrum from weaker lines outside 13–14 nm, a 141-nm thick Zr filter was used—*dotted line*. The result of the filtration is shown as a *dashed line*

For the 13.84 nm wavelength, the FWHM $\Delta\lambda$ was equal to $\sim$1 Å. This corresponds to a coherence length of $l_c = \frac{\lambda^2}{\Delta\lambda} =$ 1.94 µm.

3.3 MLM focal spot imaging with pinhole camera

Additionally, the focal spot of the EUV source was studied. The imaging was performed using a 200-nm thick Zr foil placed near the focus of the MLM collector. The position of the Zr foil was adjusted using a Standa FL42STH33 step motor with 1.25-µm step size and 13-mm travel distance. The foil acts as a screen necessary to scatter the quasi-monochromatic EUV radiation. A pinhole camera with a 32-µm diameter laser drilled pinhole was used for acquiring the focal spot images. The object and image distances were equal to 121 and 209 mm, respectively, resulting in the lateral magnification equal to $\sim$1.73. As a detector a back-illuminated CCD camera was employed, X-Vision M25 from REFLEX s.r.o., Czech Republic. The camera was equipped with a 0.5×0.5 inch^2, 512×512 pixels chip having 24.8-µm square pixels, but its resolution defined as the convolution between the geometrical shadowing and the diameter of the main Fraunhofer diffraction peak, discussed in detail in [20], was estimated to be 118 µm. The schematic description of the setup is shown in Fig. 10. The normal incidence rays that affect the intensity distribution were eliminated using a 20-mm diameter beam block installed between the collector and the Zr foil 76 mm away from the collector. An exposure of 200 shots (20 seconds) was necessary to obtain the intensity distribution near the focal plane of the MLM collector. A few examples of the intensity distributions near the focal plane, shown in Fig. 11(a–f), were acquired at the Zr foil positions −3, −2, −1, 0, 1 and 2 mm, respectively. Figure 12 shows the results of the focal spot size calculations from the image data. The diameters in the two orthogonal directions x and y, corresponding to p and s planes, respectively, were measured at FWHM for each intensity distribution and the FWHM spot area was calculated. The focal spot is elliptical with a ratio of the major and minor axes equal to 2.8 at the location of the smallest spot. This location ($z = 0$ mm) was assumed to be the focal plane of the MLM. The major and minor axes of the ellipse-shaped focal spot were measured to be equal to 1090 µm and 390 µm, respectively.

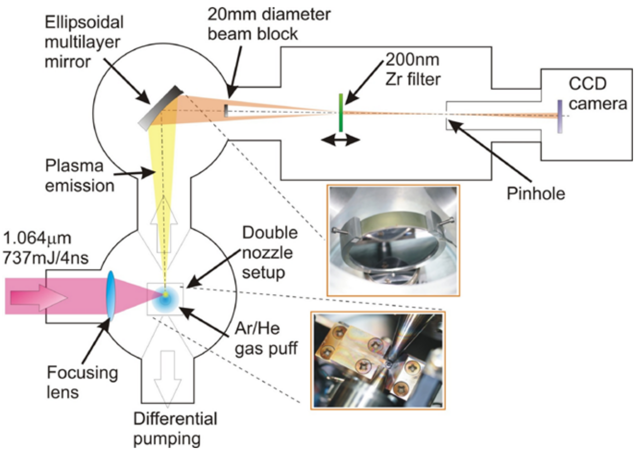

Fig. 10 Schematic of the experimental arrangement for multi-layer mirror focal spot imaging employing a pinhole camera

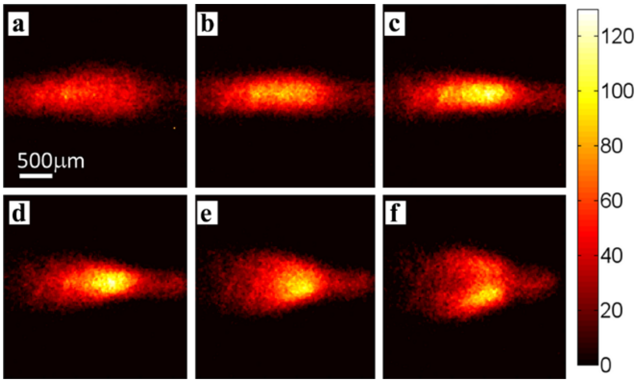

Fig. 11 Intensity distributions near the focal plane of the MLM collector (**a**–**f**) acquired at −3, −2, −1, 0, 1, and 2 mm, respectively

3.4 Mirror enhancement factor measurements

The mirror enhancement factor measures the ratio of the energy densities obtained with and without the multi-layer collector. The scheme of the experimental setup used to measure the MLM enhancement factor is shown in Fig. 13.

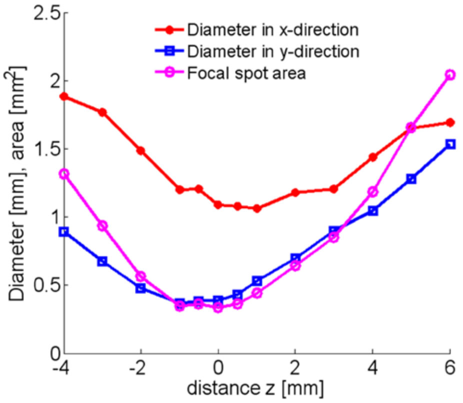

Fig. 12 Focal spot diameters in orthogonal directions and the focal spot area measured at different planes near the focal plane of the MLM collector

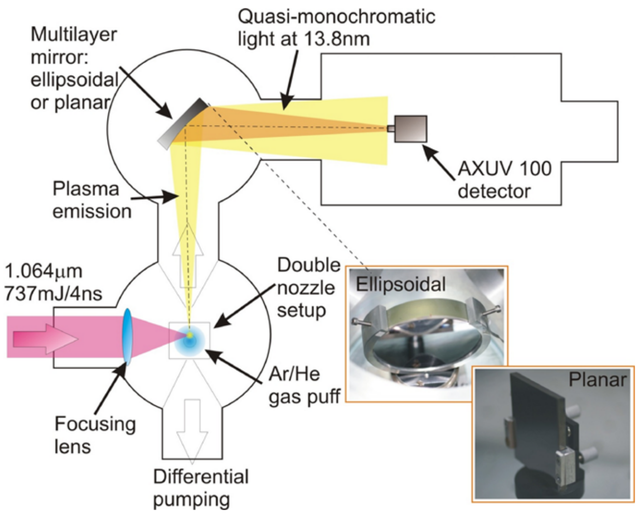

Fig. 13 Schematic of the experimental arrangement for the MLM enhancement factor measurements

The enhancement in the energy density using the MLM comes from the fact that this optic focuses the light into $\sim 1 \times 0.4\ \mathrm{mm}^2$ spot as compared to the planar mirror PM which does not change the incident wavefront. Planar and ellipsoidal mirrors were used to direct the EUV light onto the detector. It was assumed that the reflectivities of both mirrors are equal.

If the total number of photons emitted in the 13–14 nm wavelength range from the source, uniformly into 4π solid angle, is equal to N_0 then for the MLM the photon density at the detector plane can be calculated as:

$$N_e = \chi \frac{N_0 \cdot \Omega_e \cdot R_{\mathrm{MLM}}}{4\pi S_e} \tag{1}$$

where $\Omega_e = \frac{S_{\mathrm{MLM}}}{r_m^2}$ is the solid angle subtended by the MLM, r_m is the distance between the MLM and the nozzle, S_{MLM} is the area of the mirror as seen from the nozzle plane, R_{MLM} is the MLM reflectivity and S_e is the focal spot size of the MLM. If there are no obstacles between the MLM and the plasma, the χ-factor defining the "shadowing" effect of the plasma onto the MLM is equal to 1. Due to the extended size of the plasma and the 1.06 mm diameter pinhole used for differential pumping and placed 4 mm away from the plasma, our simulations estimate χ to be 0.504. This means that the horizontally elongated plasma projected onto a vertically elongated mirror (as seen from the nozzle plane for the circular MLM at 45° incidence angle) is clipped by the mirror and only 50.4% of the photons are focused by the MLM.

For the PM the photon density at the detector plane can be similarly expressed as:

$$N_p = \frac{N_0 \cdot \Omega_p \cdot R_{\mathrm{PM}}}{4\pi S_d} \tag{2}$$

where $\Omega_p = \frac{S_d}{(r_m+r_d)^2}$ is the solid angle subtended the PM, r_d is the distance between the PM and the detector, S_d is the detector area and R_{PM} is the reflectivity of the PM. In this case, the solid angle subtended by the detector Ω_p is small compared to Ω_e and the size of the pumping pinhole does not influence the number of photons collected by the detector, hence $\chi = 1$. Calculating the ratio of energy densities, one can find the theoretical mirror enhancement factor:

$$\eta_t = \frac{N_e}{N_p} = \chi \frac{\Omega_e \cdot R_{\mathrm{MLM}} \cdot S_d}{\Omega_p \cdot R_{\mathrm{PM}} \cdot S_e}. \tag{3}$$

To assess the enhancement factor experimentally, the AXUV detector was used again and the number of photons per laser shot was measured for the MLM and the PM in place. The experimental enhancement factor can be then expressed as:

$$\eta_e = \frac{N_{me} \cdot S_d}{N_{mp} \cdot S_e} \tag{4}$$

where N_{me}, N_{mp} are the numbers of photons measured for the MLM and the PM respectively.

Both mirrors studied were placed at 45° incidence angle and $r_m = 254$ mm from the gas nozzle. The AXUV 100 detector was positioned at the distance $r_d = 280.7$ mm from the center of the MLM/PM mirrors. For the PM the entire detector area is exposed to the EUV radiation in the wavelength range 13–14 nm, while for the MLM this distance assures that the detector is not exactly at the focus of the mirror, however it still collects all the focused EUV light. From the geometry, the spot size on the detector placed 26.7 mm downstream the focal plane was calculated to be $4.2 \times 2.9\ \mathrm{mm}^2$.

It was assumed that both mirrors have the same reflectivity $R_{\mathrm{MLM}} = R_{\mathrm{PM}}$. The area of the MLM placed at 45° incident angle is an ellipse $S_{\mathrm{MLM}} = \pi \cdot a \cdot b$, $a = 40$ mm, $b = a \cdot \cos(\pi/4) = 28.3$ mm. From Sect. 3.3, the focal spot size was imaged using a pinhole camera and it was found that it is an ellipse with major and minor axes equal to $d_1 = 1.09$ mm and $d_2 = 0.39$ mm, respectively, leading to the focal spot size $S_e = 0.25\pi \cdot d_1 \cdot d_2$. The number of photons per laser shot was statistically calculated based on ten consecutive measurements. At the optimized timing parameters, as discussed in Sect. 3.1, it was found that the number of photons/shot employing MLM and PM is equal to $(8.8 \pm 0.5) \times 10^{10}$ and $(1.4 \pm 0.1) \times 10^9$ respectively. Moreover, the pinhole camera resolution was estimated to be equal to ∼120 µm that affects the focal spot area equal to $S_e = 0.36 \pm 0.11$ mm^2 and the error in the detector size measurement of 20 µm leading to the detector area $S_d = 100.0 \pm 0.4$ mm^2. Based on an error analysis, the statistical σ error was estimated from these measurements. The enhancement factor was calculated to be $\eta_e = (1.9 \pm 0.6) \times 10^4$ while the theoretical enhancement factor was equal to $\eta_t = 2.4 \times 10^4$. The error between the measurements, expressed as $\frac{\eta_t - \eta_e}{\eta_t}$, is equal to 19.4%. The most probable explanation of the discrepancy between the measured and theoretical values is a ∼30-nm thick carbon layer, deposited on the MLM due to the many hundreds of hours of operation and multiple pumping/venting cycles reducing the reflectivity of the MLM by the factor equal to the error quoted above.

The photon density at the detector plane per laser shot is for the MLM equal to 2.6×10^{13} photons/cm^2 or ∼0.4 mJ/cm^2, while for the planar mirror 1.4×10^9 photons/cm^2 or 19.7 nJ/cm^2 are obtained. Enhancement of the energy density obtained by employing the MLM as a spectral selector and an efficient collector is significant from the practical point of view. For example, considering a common PMMA (polymethyl methacrylate) photoresist, its sensitivity is low and requires >500 mJ/cm^2 at 248 nm in the visible and ∼1–2 J/cm^2 at 8.3 Å in the hard X-ray region [21]. However, the sensitivity increases significantly in the EUV region and at 13.4 nm wavelength it was estimated by Junarsa et al. [22] to be equal to ∼38 mJ/cm^2. Thus employing this EUV source, it is expected that the exposure of ∼100 shots or 10 seconds is sufficient to achieve the dose required for PMMA to activate the photoresist, keeping in mind that the inverse relative bandwidth of the emission equals 140.

4 Summary and conclusions

A detailed study of the Ar-based gas-puff target source is presented. The source is capable of emitting quasi-monochromatic radiation at 13.8 nm wavelength. The source timing optimization, the energy as well as the spectral and spatial distributions of the radiation emitted from the source, and the MLM enhancement factor are studied in detail. Pulse energies up to ∼1.3 µJ/pulse at 10 Hz repetition rate are measured. Spectral measurements reveal the inverse relative bandwidth of $\lambda/\Delta\lambda \sim 140$. This debris-free gas-puff source has the potential to be used in imaging using diffractive optics, in metrology and even actinic mask inspection due to its emission near 13.5 nm wavelength. The energy density of the source of ∼0.4 mJ/cm^2 offers the possibility to employ it in lithography.

Acknowledgements The research was partially performed in the frame of the EUREKA project Σ!3892 ModPolEUV supported by the Ministry of Science and Higher Education of Poland (decision Nr 120/EUR/2007/02) and under the COST Action MP0601. We would like to thank Professor Mario C. Marconi and Professor Carmen S. Menoni from Colorado State University for their help and constructive comments during the preparation of this manuscript. P.W.W. would also like to greatly appreciate the financial support obtained from the Foundation for Polish Science, HOMING 2009 Programme, HOM2009/14, and European Economic Area (EEA) Grants.

References

1. V. Bakshi, in *Semiconductor International*, Austin, TX, March 2009
2. P.W. Wachulak, M.C. Marconi, R.A. Bartels, C.S. Menoni, J.J. Rocca, J. Opt. Soc. Am. B **25**, 1811 (2008)
3. P.W. Wachulak, L. Urbanski, M.G. Capeluto, D. Hill, W.S. Rockward, C. Iemmi, E.H. Anderson, C.S. Menoni, J.J. Rocca, M.C. Marconi, J. Micro/Nanolith. MEMS MOEMS **8**, 021206 (2009)
4. R.A. Bartels, A. Paul, H. Green, H.C. Kapteyn, M.M. Murnane, S. Backus, I.P. Christov, Y. Liu, D. Attwood, C. Jacobsen, Science **297**, 376 (2002)
5. I.J. Kim, G.H. Lee, S.B. Park, Y.S. Lee, T.K. Kim, C.H. Namb, Appl. Phys. Lett. **92**, 021125 (2008)
6. R.L. Sandberg, A. Paul, D.A. Raymondson, S. Hadrich, D.M. Gaudiosi, J. Holtsnider, R.I. Tobey, O. Cohen, M.M. Murnane, H.C. Kapteyn, C. Song, J. Miao, Y. Liu, F. Salmassi, Phys. Rev. Lett. **99**, 098103 (2007)
7. R.I. Tobey, M.E. Siemens, O. Cohen, M.M. Murnane, H.C. Kapteyn, K.A. Nelson, Opt. Lett. **32**, 3 (2007)
8. G. Vaschenko, C. Brewer, F. Brizuela, Y. Wang, M.A. Larotonda, B.M. Luther, M.C. Marconi, J.J. Rocca, C.S. Menoni, Opt. Lett. **31**, 9 (2006)
9. T. Teresawa, T. Yamane, T. Tanaka, T. Iwasaki, O. Suga, T. Tomie, in *Proceedings of SPIE, the International Society for Optical Engineering, Alternative Lithographic Technologies*, San Jose, CA, 24–26 February 2009
10. H. Fiedorowicz, A. Bartnik, R. Jarocki, M. Szczurek, T. Wilhein, Appl. Phys. B **67**, 391 (1998)
11. P.W. Wachulak, A. Bartnik, H. Fiedorowicz, P. Rudawski, R. Jarocki, J. Kastecki, M. Szczurek, Nucl. Instrum. Methods Phys. Res. B **268**, 1692 (2010)
12. H. Fiedorowicz, A. Bartnik, R. Jarocki, R. Rakowski, M. Szczurek, Appl. Phys. B **70**, 305 (2000)
13. A. Bartnik, H. Fiedorowicz, R. Jarocki, L. Juha, J. Kostecki, R. Rakowski, M. Szczurek, Appl. Phys. B **82**, 529 (2006)
14. A. Bartnik, H. Fiedorowicz, R. Jarocki, J. Kostecki, R. Rakowski, M. Szczurek, Appl. Phys. B **93**, 737 (2008)
15. A. Bartnik, H. Fiedorowicz, R. Jarocki, J. Kostecki, A. Szczurek, M. Szczurek, Appl. Phys. B **96**, 727 (2009)

16. H. Fiedorowicz, A. Bartnik, R. Jarocki, J. Kostecki, J. Krzywinski, J. Mikołajczyk, R. Rakowski, A. Szczurek, M. Szczurek, J. Alloys Compd. **401**, 99 (2005)
17. C.X.R.O. X-Ray Interactions, With Matter: http://henke.lbl.gov/optical_constants/
18. Manufacturer's specification: http://www.ird-inc.com/axuvwdd/axuv_ti_zr_c.html as in August 2009
19. R.L. Kelly, J. Phys. Chem. Ref. Data **16**(Suppl. 1) (1987)
20. B. Yang, in *BIW'02*. AIP Proc., vol. 648, pp. 59–78 (2002)
21. http://www.microchem.com/products/pdf/PMMA_Data_Sheet.pdf, PMMA datasheet
22. I. Junarsa, M.P. Stoykovich, P.F. Nealey, Y. Ma, F. Cerrina, H.H. Solak, J. Vac. Sci. Technol. B **23**, 138 (2005)